Published in final edited form as:

J Mol Cell Cardiol. 2018 January ; 114: 161–174. doi:10.1016/j.yjmcc.2017.11.012.

Resident fibroblast expansion during cardiac growth and remodeling

Malina J. Ivey[1,2,**], **Jill T. Kuwabara**[1,2,**], **Jonathan T. Pai**[1], **Richard E. Moore**[3], **Zuyue Sun**[1], and **Michelle D. Tallquist**[1]

[1]Center for Cardiovascular Research, John A. Burns School of Medicine, University of Hawaii at Manoa, Honolulu, HI 96813

[2]Department of Cell and Molecular Biology, John A. Burns School of Medicine, University of Hawaii at Manoa, Honolulu, HI 96813

[3]Department of Molecular Biochemistry and Bioengineering, John A. Burns School of Medicine, University of Hawaii at Manoa, Honolulu, HI 96813

Abstract

Cardiac fibrosis, denoted by the deposition of extracellular matrix, manifests with a variety of diseases such as hypertension, diabetes, and myocardial infarction. Underlying this pathological extracellular matrix secretion is an expansion of fibroblasts. The mouse is now a common experimental model system for the study of cardiovascular remodeling and elucidation of fibroblast responses to cardiac growth and stress is vital for understanding disease processes. Here, using diverse but fibroblast specific markers, we report murine fibroblast distribution and proliferation in early postnatal, adult, and injured hearts. We find that perinatal fibroblasts and endothelial cells proliferate at similar rates. Furthermore, regardless of the injury model, fibroblast proliferation peaks within the first week after injury, a time window similar to the period of the inflammatory phase. In addition, fibroblast densities remain high weeks after the initial insult. These results provide detailed information regarding fibroblast distribution and proliferation in experimental methods of heart injury.

Keywords

cardiac fibroblast; endothelial cell; proliferation; fibrosis

Correspondence to: Michelle D. Tallquist.

[**]These authors contributed equally to this work.

Disclosures

None.

1. Introduction

Cardiac fibrosis is a hallmark of cardiovascular disease and is associated with fibroblast proliferation. After injury, the accepted role of the cardiac fibroblast is to replace dying cardiomyocytes with extracellular matrix (ECM) [1], and inhibition of fibroblast expansion results in heart rupture [2–4]. Although fibrosis is a key element of heart pathogenesis [5], our understanding of the biology of the cardiac fibroblast is rudimentary. One major limitation has been the inability to identify these cells in vivo. The study of cardiac fibroblasts has been, to some degree, restricted to in vitro analysis or to investigation of an activated fibroblast population known as the myofibroblast. The myofibroblast is a fibroblast sub-type that was traditionally identified by expression of α-smooth muscle actin (αSMA, ACTA2) [6] and is considered the prototype for understanding fibroblast function [7]. While these data have been extremely informative, recent observations suggest that myofibroblasts represent only a portion of the matrix-producing, proliferative fibroblasts [2, 4, 8]. It is possible that the majority of fibroblasts responsible for the fibrotic response have been largely ignored. Therefore, a reevaluation of fibroblast biology using more inclusive and definitive means of identification will help to clarify the influence of fibroblasts during cardiac fibrosis.

A lack of specific markers has also impeded a consensus regarding cardiac fibroblast numbers and function. We have recently demonstrated that during homeostasis resident cardiac fibroblasts constitute a smaller proportion of cardiac cells than previously believed [9]. Additionally, it was thought that activated fibroblasts were heterogeneous and derived from different sources after injury. However, recent evidence points to the resident fibroblast as the main source of ECM producing fibroblasts during ventricular remodeling [2, 8, 10]. Resident fibroblasts can be defined by expression of PDGFRα and type I collagen, as well as deriving from the Tcf21 lineage [8–11], while activated cardiac fibroblasts have been recently classified by periostin expression [2, 4].

Even though fibroblasts contribute to important aspects of heart development, physiology, and pathology, little is known about the in vivo proliferative behavior of the resident fibroblast. In the past, mapping of resident fibroblasts has been approximated using transmission electron microscopy [12] or markers that are enriched but not specific to fibroblasts [13]. To provide a comprehensive view of the distribution and proliferation of cardiac fibroblasts, we have employed four distinct fibroblast tracking mouse lines to define the proliferation rates at three stages: early postnatal, adult, and after cardiac injury.

Our findings demonstrate that during early postnatal growth fibroblasts and endothelial cells proliferate in a profile similar to that of cardiomyocytes [14–16]. In addition, using three distinct experimental injury techniques, we observed grossly different spatial patterns of fibroblast expansion. Furthermore, regardless of the injury type, fibroblast proliferation rates peaked rapidly within the first week and returned to basal levels, suggesting a limited time frame for the proliferative phase. These findings provide important insights regarding fibroblast proliferation in the heart and provide a foundation for future studies involving fibroblast activation and regulation after cardiac injury.

2. Materials and Methods

2.1 Mice

Tcf21$^{mCrem/+}$ [17], *PDGFRα*$^{GFP/+}$ [18] (Jackson Labs, 007669), *Collagen1a1-GFP* [19], *POSTN*$^{mCrem/+}$ [2] and *R26R*^{tdT} [20] (Jackson Labs, 007914) have been previously described. All animal protocols and experiments were approved by the University of Hawaii at Manoa IACUC and conformed to National Institutes of Health guidelines for care and use of laboratory animals. Mice were backcrossed a minimum of four generations to C57BL/6J and contained the J mutation of the NNT gene. Both males and females were used for these studies.

2.2 Tamoxifen inductions

Tamoxifen (MP Biomedicals, 0215673891) was administered to mice by oral gavage (0.3 mg/g body weight) two or three times on non-consecutive days or 250 mg/kg of sucrose tamoxifen chow (Harlan Laboratories) for 14 days in *Tcf21*$^{mCrem/+}$ mice. For postnatal inductions of *Tcf21*$^{mCrem/+}$ mice, tamoxifen (100–500 μg) was injected intragastrically between postnatal days 2–4. No reporter activity was detected at any time in the absence of tamoxifen. For induction of the *POSTN*$^{mCrem/+}$ mice, a single oral gavage of tamoxifen (10 mg) was administered 1 or 3 days after injury.

2.3 Immunostaining and microscopy

Hearts were isolated at the selected time points and fixed with freshly prepared 4% paraformaldehyde (PFA) in DPBS for 1 hour at room temperature or overnight at 4°C, cryoprotected in 30% sucrose/DPBS for two hours, and embedded in OCT. Immunostaining was performed on 10 μm tissue sections, treated with 0.1% Triton-X-100/DPBS, or 0.5% Triton-X-100/DPBS for αSMA staining, for 30 min and blocked with 1% BSA/DPBS. Tissue staining was performed overnight. For list of antibodies and reagents see Supplemental Table 1. When necessary, secondary antibodies from Thermofisher were used at a 1:500 concentration for 1 hour at room temperature. Nuclei were stained with DAPI (Roche, 10-236-276-001). A Zeiss Axiovert 200 microscope equipped with an Olympus DP71 camera was used for imaging. Images were edited and figures were created in Photoshop CS6.

2.4 Cardiac fibroblast quantification

Cardiac fibroblast cell number was quantified by counting the number of tdTomato^{+} or GFP^{+} cells identified by DAPI^{+} nuclei using the ImageJ cell counter plugin and normalized to myocardial area, DAPI area, or DAPI^{+} nuclei as specified in figure legends. Percent of myocardial or DAPI area was calculated by converting the image to black and white using threshold color and analyzing particles using ImageJ. Specific methods of quantification for each experimental group are described in detail below.

2.5 Survival Surgeries

Adult mice older than 6 weeks and >22.0 g were subjected to either pressure overload by transverse aortic constriction (TAC), myocardial infarction (MI) by permanent ligation of the

left anterior descending artery (LAD), or subcutaneous isoproterenol injections following protocols approved by the University of Hawaii Animal Care and Use Committee. Surgeries were performed by the Cardiovascular Center Mouse Phenotyping Core.

2.5.1 TAC—Animals were anesthetized using isoflurane (2% in O_2) followed by endotracheal intubation and ventilation with 1–2% isoflurane on an Inspira Advanced Safety Ventilator (Harvard Apparatus, Holliston, MA, USA). A partial thoracotomy was performed to expose the transverse aorta between the brachiocephalic and left common carotid artery by microsurgical techniques. A 6.0 silk suture was placed between the innominate and left carotid arteries and around the ascending aorta. A 26-gauge blunted needle was placed parallel to the aorta under the suture, two knots were tied and needle removed. Sham operations were performed in the same manner, but the suture was removed instead of tied.

One week after TAC or sham surgery, mice were anesthetized with 1–2% isoflurane and Doppler echocardiography was performed to confirm and measure the level of constriction. A Visualsonics Vevo 2100 system with MS550 transducer (32–56MHz) was used. The aortic arch view was obtained from a right parasternal view, and the pulsed wave Doppler sample volume was placed in the transverse aorta just proximal and distal to the site of banding. The waveforms of aortic flow across the constriction site were traced using Vevo 2100 software. Successful TACs were identified by increased flow velocity downstream of the constriction site (typically around 3 to 4 m/sec in TAC mice). Pressure gradient across the constriction was calculated based on peak flow velocity according to a modified Bernoulli's equation.

2.5.2 Isoproterenol treatment—Mice were subjected to cardiac damage by subcutaneous injection of isoproterenol (TCI, I0260) or saline for 2 to 14 consecutive days at a dose of 50 mg/kg of body weight.

2.5.3 MI—A thoracotomy was performed between the third and fourth rib to expose the LAD artery. The LAD proximal artery was permanently ligated using a 7.0 silk suture. Ligation was confirmed by visualization of left ventricle (LV) blanching and ST elevation on the electrocardiogram. Sham animals underwent the exact surgical procedure, except the suture was not tied and was removed prior to closing the thoracic cavity.

2.6 Echocardiography

Echocardiograms and tissue Doppler imaging (TDI) were performed to analyze baseline levels and effectiveness of TAC and MI surgeries. Briefly, hair removal cream was applied to the chest until all fur was removed from the area. A layer of ultrasound gel was applied to the animal’s chest, and the probe was lowered parasternally at 90° between the probe and the heart. B- and M-modes were performed to record 2-dimensional and 1-dimensional transverse cardiac measurements and used to analyze left ventricular function.

2.7 Proliferation assay

5-ethynyl-2'-deoxyuridine (EdU; Santa Cruz, sc-284628) was administered by IP injection (50 mg/kg body weight) 24 hours before isolation. Hearts were processed for histological analysis as described above and stained using Click-iT EdU Alexa Fluor Imaging Kits

(Molecular Probes, C10637 and C10337) according to the manufacturer's protocol. Flow cytometry analysis is described below.

2.7.1 Postnatal proliferation—For postnatal analysis, the total percent of EdU^+ cells was calculated by EdU^+ cells divided by total number of $DAPI^+$ cells in a 40× field of view (FOV). Fibroblast proliferation index was calculated by dividing the number of double positive $tdTomato^+$ or GFP^+ cells with EdU by the total number of $tdTomato^+$ or GFP^+ cells in a 20× FOV. Endothelial proliferation index was calculated by dividing the number of double positive $IB4^+$ cells with EdU by the total number of $IB4^+$ cells in a 20× FOV. Between 7–20 FOV were quantified per heart.

2.7.2 Transverse aortic constriction (TAC) proliferation—For TAC proliferation, lesions were defined by an accumulation of >50 $tdTomato^+$ fibroblasts in a 40× FOV, and 18–20 lesions were quantified per time point. Adventitial lesions were defined by $tdTomato^+$ fibroblast accumulation around a blood vessel. Interstitial lesions were identified by $tdTomato^+$ fibroblasts in the myocardium of the LV. Fibroblast proliferation index was calculated by dividing the number of EdU^+ fibroblasts by the total number of fibroblasts in lesion and non-lesion areas.

2.7.3 Isoproterenol proliferation—For isoproterenol proliferation, 5–12 20× FOV from the LV and interventricular septum (IVS) endocardium were used to determine proliferation index. Fibroblast proliferation index was calculated by dividing the number of EdU^+ fibroblasts by the total number of fibroblasts within the endocardium. The fraction of proliferating cells that are fibroblasts was calculated by dividing the number of EdU^+ fibroblasts by the total number of EdU^+ cells in the endocardium. The number of fibroblasts and the number of proliferating cells was calculated by normalizing to myocardial area and determining the average of each section and then each heart. Two or more non-sequential sections per heart, and two or more biological replicates were compared at each time point and region post-surgery.

2.7.4 Myocardial infarction (MI) proliferation—For MI proliferation, 2–6 20× FOV were used to determine proliferation index of each infarct. The number of FOV was dependent on infarct size. To determine border proliferation, 2–3 20× FOV were taken from the edges of the infarct, utilizing the difference in autofluorescence between the infarct and adjacent myocardium as a guide (SFigure 5I–K). Border was defined as ~50% of the myocardium in that FOV as having a decreased autofluorescence and loss of cardiomyocytes. Proliferation in the remote area was calculated from 2–4 20× FOV of uninjured right ventricle tissue in the same section as the infarct and border quantifications. For sham surgeries, >10 FOV were used per section. MI proliferation indexes were calculated as described for isoproterenol proliferation. Both the number of fibroblasts and the number of proliferating cells were calculated by normalizing to the DAPI area. DAPI area, rather than myocardial area, was used to avoid inclusion of acellular regions and dead cardiomyocytes in severe infarcts. Two or more non-sequential sections per heart and two or more biological replicates were compared at each time point and region post-surgery.

2.8 Trichrome staining

Trichrome staining was performed on frozen sections using Gomori Trichrome Stain Kit (VWR, 84000-308) according to the manufacturer's recommendations.

2.9 Flow cytometry

Adult murine hearts (>6 weeks of age) were perfused with DPBS containing 0.9mM Ca^{2+} and were dissected. Atria and valves were removed. For isoproterenol analyses, whole ventricles were used for baseline and injury samples. For MI analyses, infarct regions were identified by blanching and accumulation of Col1a1-GFP^{+} or PDGFRα^{GFP+} fibroblasts and excised. The remaining tissue was used for border/remote analyses. For MI baseline analysis left ventricle was substituted for infarct. Tissue weight was determined before digestion. Single cell suspensions were obtained as previously described [9]. Briefly, tissue was minced and incubated with collagenase type IV (600 U/ml, Worthington, LS004188) and dispase II (1.2 U/ml, Thermofisher, 17105041) in DPBS containing 0.9mM Ca^{2+} for 45 min at 37°C and filtered through both a 40μm and 30μm filter. Single cell suspensions were incubated with fixable yellow dead cell stain (1:1000, Molecular Probes, L34959) for 30 min at 4°C and washed in 2% FBS/DPBS. Cells were then incubated in primary antibodies (STable 1) in 2% FBS/DPBS for 30 min at room temperature, washed, and fixed for 15 min in freshly made 4% PFA/DPBS. EdU labeling was performed using a Click-iT Plus EdU Alexa Fluor Imaging Kit (Molecular Probes, C10636) according to the manufacturer's protocol. Cells were washed with 1% BSA to stop the EdU reaction. For samples with αSMA staining, cells were incubated with an αSMA antibody (STable 1) or an isotype control (BD Pharmingen, 555574) in 1% BSA/DPBS for 30 minutes at room temperature, washed, and resuspended in 1% BSA/DPBS and Accucheck counting beads (Thermofisher, PCB100) according to the manufacturer's protocol. Compensation beads (eBioscience, 01-2222-42) were used for antibody compensation analysis and data were compensated and acquired on a LSRFortessa (BD Bioscience). Gating analyses were performed using FlowJo (TreeStar), and cell counts were calculated according to the Accucheck counting bead manufacturer's recommendations.

2.10 Statistical analysis

All statistical analyses were conducted using Prism 5 (Graphpad Software, Inc., La Jolla, USA). Statistical analyses between two groups were analyzed using unpaired student's t-test. Comparisons between fibroblast proliferation groups were analyzed using one-way ANOVA with Tukey test (Supplemental Tables 2–4). Statistical variability is expressed as mean ± SD.

3. Results

3.1 Cardiac fibroblast distribution

Using four independent mouse lines, we have characterized fibroblast location and proliferation during heart growth and after injury. Each of these lines identifies fibroblasts using different cis-regulatory elements and temporal expression. The *Col1a1-GFP* transgenic line expresses a cytoplasmic GFP under the control of a *Col1a1* enhancer/promoter and

identifies resting resident cardiac fibroblasts [8, 19, 21]. *PDGFRα*^{GFP}, a targeted nuclear GFP insertion at the *PDGFRα* locus labels a majority of cardiac fibroblasts [9, 18, 21, 22]. Additionally, two tamoxifen inducible Cre lines were used to track relevant fibroblast populations and their progeny. Resting and activated fibroblasts can be indelibly labelled using *Tcf21*^{mCrem} [9, 17] and *POSTN*^{mCrem} [2], respectively. These Cre lines were crossed to a recombination sensitive reporter, *R26R*^{tdT} [20], to lineage trace cardiac fibroblasts. Figure 1 demonstrates labeling of fibroblasts in the uninjured heart. The three lines that label resident cardiac fibroblasts identify strikingly similar populations of cells in the ventricles as previously reported [9]. To further delineate the fibroblast populations designated by the GFP lines, we crossed the mice expressing the two GFP-expressing alleles and examined overlap in heart sections. SFigure 1A demonstrates that a majority of the fibroblasts identified in *Col1a1-GFP* hearts also contained nuclear-localized GFP from the *PDGFRα*^{GFP} allele. In addition, quantification of GFP$^+$ cells by flow cyotometry also revealed a similar total content of GFP$^+$ cells when comparing *Col1a1-GFP* and *PDGFRα*^{GFP} hearts (SFigure 1B). We also examined the expression of other fibroblast markers within these two strains. In both mouse lines, GFP$^+$ cells also co-expressed vimentin (SFigure 2A–B). We also noted that vimentin was expressed in mural cells surrounding coronary arteries. By contrast, DDR2 expression did not correspond well with GFP$^+$ fibroblasts (SFigure 2C–D). Instead, DDR2 expression overlapped with a pericyte marker (NG2) and to a lesser extent with an endothelial cell marker (isolectin B4, IB4) (SFigure 2E–H). As previously reported [9], flow cytometry demonstrated that greater than 95% of the GFP$^+$ cells from either fibroblast line were MEFSK4$^+$ whereas Sca1 and Thy1 were expressed more heterogeneously (data not shown). GFP$^+$ cells were also negative for smooth muscle cell marker (αSMA), pericyte marker (CD146), mesenchymal stem cell markers (CD44 and CD166) [23–25] at baseline by flow cytometry (Figure 3G–H and data not shown.)

While *PDGFRα*^{GFP} and *Col1a1-GFP* are also expressed in adventitial fibroblasts of the aorta, a limited number of Tcf21 lineage labeled cells were found in the adventitia distal to the aortic valve (data not shown). In mice that were tamoxifen treated within the first week after birth, Tcf21 lineage labeled cells were less frequent in the IVS (Figure 1C and SFigure 3E), where endothelial-derived fibroblasts reportedly predominate [8, 10]. Cells in the atria (Fig 1A–C and SFigure 3A), aortic, pulmonary, tricuspid, and mitral valves and epicardium (data not shown) were also marked. Before injury, Tcf21 lineage labeled cells are uniformly positive (>95%) for vimentin, MEFSK4, and GFP from *Col1a1-GFP* and *PDGFRα*^{GFP} mice (manuscript in preparation). It is to be noted that the ability of Tcf21^{mCrem} to recombine in fibroblasts is dependent on the efficiency of tamoxifen induction, and we find that we can routinely tag ~60–70% of the fibroblasts with adult tamoxifen inductions (manuscript in preparation). Given the ability to track fibroblasts with these lines, we further examined fibroblast localization and proliferation during postnatal development and after heart injury.

3.2 Postnatal fibroblast proliferation

Immediately after birth, the heart undergoes key developmental changes that are marked by exponential increases in volume and cell number. While recent papers have carefully examined the proliferation and hypertrophy of cardiomyocytes during perinatal heart growth

[15, 26, 27], data on the expansion of other cell populations is limited. As endothelial cells have been shown to outnumber all other non-myocytes in the heart [9], we tracked both perinatal fibroblast and endothelial cell proliferation. To investigate the proliferation rates of fibroblasts and endothelial cells, we used EdU to track cell proliferation in three mouse lines. The aforementioned fibroblast lines were used to track fibroblasts and IB4 binding was used to designate endothelial cells. Both the *PDGFRα*^{GFP} and *Col1a1-GFP* mouse lines have reporter activity in postnatal fibroblasts (Figure 2A and data not shown). First, we determined the overall proliferation rate of cells in the LV of the heart and found that at postnatal day 2 (P2) over 10% of the cells have replicated DNA while this value increased to 15–20% of the cells at P4 and P7. After P7, EdU incorporation dramatically decreased. These data are in agreement with previous observations [15, 27, 28] (Figure 2A–B). Fibroblasts and endothelial cells represent only a subset of the total proliferating cell population in the first week after birth (Figure 2A). The total number of EdU^{+} endothelial cells outnumbered fibroblasts at each time point examined. This result likely reflects the fact that overall there are more endothelial cells than fibroblasts as the proliferation index of both cell types was similar (Figure 2C–D). These data were consistent regardless of the mouse line used to identify fibroblasts. Tcf21 lineage traced cells exhibited slightly lower proliferation rates, which could be a technical issue as only a single dose of tamoxifen was administered. By 3 weeks after birth, fibroblast and endothelial cell proliferation rates were reduced (Figure 2C–D), and the fibroblast proliferation rate (0.36 ± 0.22%) was equivalent to that observed in adult hearts (described below). Taken together, these data suggest that non-myocyte proliferation rates peak in the first week of postnatal growth, which also follows the reported pattern of cardiomyocyte proliferation [14–16], and decreases to adult levels by 3 weeks of age.

3.3 Patterns of fibroblast expansion after injury

Often ECM production is used to follow cardiac fibroblasts after injury. It is assumed that the fibroblast population expands prior to the deposition of ECM, but little is known regarding the numbers and localization of the fibroblasts. While matrix accumulation can yield important information regarding fibroblast presence, it may be that not all fibroblasts are actively producing matrix or located in areas of dense collagen, and collagen deposition may over-represent the fibroblast population. To obtain a better perspective on fibroblast quantity and location after injury, we examined fibroblast lineage distribution using three different cardiac injury methods: pressure overload by TAC, β-adrenergic cardiac stress induced by isoproterenol treatment, and MI by permanent ligation of the LAD artery. The *Col1a1-GFP* and *PDGFRα*^{GFP} lines have been used to track cardiac fibroblasts after TAC [8] and cardiotoxicity [29], respectively, and these populations also expand with the aforementioned injury techniques (Figure 3A–C). Using Tcf21 lineage marking to label resident fibroblasts prior to injury [11], we were able to focus on the expansion of resident cardiac fibroblasts. Resident cardiac fibroblasts expanded following each experimental heart injury (Figure 3D–F). Similar patterns of fibroblast expansion were seen after heart injury in *PDGFRα*^{GFP} and *Col1a1-GFP* mice (Figure 6A, 7A–B and data not shown). Gomori trichrome stain revealed that areas of collagen deposition correlated with areas containing the highest concentration of lineage traced fibroblasts (Figure 4).

αSMA is commonly used to identify fibroblasts that have become activated [30]. Using the three mouse lines, we examined marked cells for αSMA expression after injury by IHC and flow cytometry. Two cell populations expressed αSMA expression after injury, coronary vascular smooth muscle cells and fibroblasts. We found that all three fibroblast marking lines had overlap with αSMA expressing cells that were not in vascular smooth muscle cell compartments (Figure 3A–F). Consistent with reports from others [2, 8], not all fibroblasts in lesion areas exhibited detectable levels of αSMA by IHC, but by flow cytometry, a majority of the Col1a1-GFP^{+} and PDGFRα^{GFP+} cells were positive for αSMA expression in the infarct region after MI (Figure 3K–L). MI border/remote areas, isoproterenol treated hearts, and TAC had fewer αSMA^{high} expressing fibroblasts (Figure 3M–N, I–J, and data not shown). Conversely, in the absence of injury 5.9% ± 4.6% of αSMA expressing cells were GFP^{+} (n=2 *PDGFRα^{GFP}* and n= 2 *Col1a1-GFP*). Five days after LAD permanent ligation 89% ± 1.6% of αSMA expressing cells in the infarct were GFP^{+} (n=2 *PDGFRα^{GFP}* and n=3 *Col1a1-GFP*). After 7 days isoproterenol treatment, 61% ± 21% of αSMA expressing cells were GFP^{+} (n=2 *PDGFRα^{GFP}* and n=2 *Col1a1-GFP*). It should be noted that after isoproterenol treatment there were fewer αSMA^{+} cells than after MI, and some of the αSMA^{+} cells from this whole ventricle isolation were likely to be coronary vascular smooth muscle cells (data not shown). MEFSK4 continued to stain the fibroblasts marked by these three mouse lines after TAC, isoproterenol, and MI (data not shown), however, MEFSK4 flow cytometry must be performed in conjunction with CD45 and CD146 as it also identifies sub-populations of immune cells and pericytes [9]. Interestingly, Sca1 expression appeared to be down-regulated after injury (data not shown). 3–10% of the Col1a1-GFP^{+} cells were CD146^{+} after MI and isoproterenol treatment, while very few of the PDGFRα^{GFP+} cells were CD146^{+} independent of the injury (data not shown).

Although the three mouse lines used to follow fibroblasts appeared interchangeable in regards to their ability to identify resident fibroblasts, each injury type resulted in a characteristic and distinct pattern of fibroblast accumulation. After pressure overload, fibroblast accumulation is most obvious in arterial adventitia (Figure 4A, G) but small focal concentrations of fibroblasts can be found in the interstitium as early as 5 days after TAC (Figure 5A). By comparison, chronic subcutaneous isoproterenol administration resulted in an expansion of fibroblasts in endocardial areas of the ventricles and IVS as previously described [31, 32] (Figure 4B, 4H, 6A, and SFigure 3G). Permanent ligation of the LAD artery predictably resulted in expansion of fibroblasts in the LV free wall distal to the ligation. Depending on proximity of the LAD ligation, fibroblast accumulation could be observed in the IVS and right ventricular free wall (Figure 4C, 4I, and SFigure 3H). Resident fibroblast numbers increased steadily in the infarct region after injury (Figure 7E–H). After chronic pressure overload, we observed that rather than scattered intermittently between cardiomyocytes, fibroblasts adopted a denser, perivascular (SFigure 4A–B) and perimysial location (SFigure 4C–D). This pattern of fibroblasts was also observed with other modes of injury after 1–2 weeks (data not shown), but not in age-matched control hearts. Another common feature that correlated with decreased heart function in the TAC and isoproterenol models was an expansion of fibroblasts in the left atria (SFigure 3B–C and data not shown). Taken together, these data suggest fibroblast expansion correlates with matrix deposition in distinct patterns which are specific to each manner of injury.

3.4 Fibroblast proliferation after TAC

Recent studies have indicated that resident cardiac fibroblasts are the predominant fibroblast population responding to pressure overload by TAC [8, 10]. Despite the fact that pressure overload leads to hypertrophy throughout the LV, fibroblast accumulation occurs in focal areas (Figure 5A). To determine if proliferation is the cause of focal fibroblast accumulation, we examined proliferation rates of Tcf21 lineage traced fibroblasts in lesion (>50 fibroblasts/40× FOV) and non-lesion areas. First, we observed that fibroblast proliferation rates did not increase until 5 days post-surgery and declined by two weeks (Figure 5B). When comparing fibroblast proliferation in lesion and non-lesion areas, we observed a trend towards higher proliferation rates in lesions, although these differences were not statistically significant. We observed similar rates of proliferation regardless if lesions were adventitial or interstitial (Figure 5C). Comparison of time point differences are provided in STable 2. These data suggest that focal expansion of fibroblasts may be a stochastic event that depends predominantly on the initial abundance of fibroblasts in a location.

3.6 Proliferation after acute β-adrenergic receptor stimulation

After subcutaneous injection of isoproterenol, fibroblasts expand and deposit collagen in the subendocardial space (Figures 4B,E, 6A, and SFigure 3G). Using Tcf21 lineage tagging to identify resident cardiac fibroblasts, we followed fibroblast proliferation after isoproterenol administration. Focusing specifically on fibroblasts in the endocardium, we observed increases in fibroblast proliferation rates in the first week (Figure 6B–E). Despite continuous isoproterenol administration, the proliferation of resident fibroblasts dropped to basal levels by two weeks (Figure 6E), and fibroblast numbers remained steady (Figure 6F). Fibroblast proliferation follows the trend of overall proliferation within the endocardium (Figure 6G). Comparison of time point differences are provided in STable 3. Even at day 7, resident fibroblasts accounted for less than 50% of the proliferating cells and the overall number of fibroblasts were at steady state between day 4 and 14 (Figure 6H). At every time point examined, regions of the myocardium that were distal to these endocardial lesions exhibited a proliferation index similar to basal levels (data not shown).

3.7 Fibroblast proliferation after MI

Although recent data using Col1a1-GFP and Wt1 lineage tracing has suggested that resident fibroblasts constitute the majority of the fibroblast cells after TAC [8, 10], there has been some suggestion that extra-cardiac fibroblasts are recruited after other types of heart injury [33, 34]. We therefore examined PDGFRα^{GFP}, Col1a1-GFP, Tcf21 lineage, and periostin lineage tagged fibroblasts after LAD ligation. Infarct regions are replete with cells identified by these four fibroblast tagging systems (Figure 7A–D). Patterns of PDGFRα^{GFP}, Col1a1-GFP, Tcf21, and periostin lineage cells were similar in the infarct areas, and as previously documented [2] the majority of cells labeled by *POSTN*^{mCrem} recombination did not extend beyond the border zones. Therefore, analyses using this line were limited to the infarct region.

To identify the profile of proliferation within the infarct, EdU incorporation was quantified in resident and activated fibroblasts. When examining all cells within the infarct the peak proliferation rate occurs within the first 7 days after permanent ligation and steadily declined

to near basal levels by 21 days after LAD ligation, although fibroblast numbers remain steady (Figure 7E–H). The profile of fibroblast proliferation follows that of overall proliferation rates (Figure 7I–J). Comparison of time point differences are provided in STable 4. Fibroblasts constituted only 20–50% of the proliferating cells within the infarct (Figure 7K). Others have suggested that fibroblast proliferation occurs in regions remote to the ischemic tissue [35, 36]. Indeed, as early as 3 days after LAD ligation, fibroblasts in remote areas were also proliferating and continued to proliferate albeit at a reduced rate compared to infarct fibroblasts (SFigure 5A–D). As might be expected the proliferation rates of fibroblasts in the border region were slightly higher than remote rates and localized next to the infarct (SFigure 5E–H). IHC staining for CD45 expressing cells in MI demonstrates that immune cells constitute a portion of the proliferating cells after MI (SFigure 6). Similarly, $CD45^+/EdU^+$ cells were observed in TAC and isoproterenol treated hearts (SFigure 6).

3.8 Flow cytometry of proliferating cells after MI

While fibroblasts are one population of proliferating cells in the heart, the majority of the EdU^+ cells were not labeled by fibroblast markers (Figure 7K). As flow cytometry permits examination of multiple cell populations simultaneously, we evaluated the number and proliferation of fibroblasts, endothelial cells, and immune cells from uninjured and ischemic hearts. Before injury, endothelial cells ($CD31^+$) constituted the overall majority of cells and the majority of the EdU^+ cells (44.9% ± 4.41%), and fibroblasts (Col1a1-GFP^+) represented only a small proportion of EdU^+ cells (2.27% ± 0.93%) (Figure 8A, E). The basal proliferation rate of fibroblasts in the uninjured heart (0.37% ± 0.17%, n=5) (Figure 8B) was similar to that observed at postnatal day 21 (0.36% ± 0.22% n=9) (Figure 2C) and in saline treated adult animals (0.40% ± 0.37%) (Figure 6E).

After LAD ligation, fibroblast numbers increased 3–4-fold, while immune cell numbers ($CD45^+$) initially increased at 5 days but decreased by 9 days (Figure 8A). The proliferation of cells in regions outside of the infarct follows similar trends (SFigure 5P). Additionally, the number of fibroblasts corresponded to the amount of ischemic area, and the number of immune cells generally correlated with the number of fibroblasts (data not shown). Using all three fibroblast marking mouse lines, we observed no significant differences of cell numbers or proliferation rates. Endothelial cells by contrast were dramatically reduced in infarct areas but are similar to basal levels in non-infarct areas (Figure 8A and SFigure 5O). In agreement with the immunohistochemistry results shown in Figure 7E–G,I, EdU^+ cells were most abundant around day 5 (Figure 8A). However, at 5 days post-MI, fibroblasts and immune cells represent the majority of the proliferating cells (37.37 ± 13.68% and 38.37 ± 3.88%, respectively) (Figure 8E). The overall number of proliferating cells decreased by 9 days post-MI, but immune and endothelial cells continued to constitute the majority of the proliferating cells (51.38 ± 15.28% and 20.68 ± 6.70%, respectively), whereas fibroblasts represent a smaller proportion (12.95 ± 6.11%) (Figure 8E). The proliferation indices of fibroblasts, immune cells, and endothelial cells within the infarct were similar at day 5. While immune cell proliferation remained relatively constant between days 5 and 9, fibroblast and endothelial cell proliferation decreased by day 9 (Figure 8B). Similar to results observed by immunohistochemistry quantification, the proliferation rate of

fibroblasts in the IVS and right ventricle were slightly increased over basal levels but were highly variable (SFigure 5O–P). Similar increases over basal levels were observed in immune and endothelial cells in non-infarct regions (SFigure 5O–P). In an attempt to identify the GFP^-, $CD45^-$, $CD31^-$ proliferating cell population, we co-stained for pericyte marker CD146. $CD45^-$, $CD31^-$, GFP^-, $CD146^+$ cells represented only 1–4% of the proliferating cells after MI (data not shown). We also did not observe an appreciable number of Sca^+, $CD44^+$, or $CD166^+$ cells in the GFP^-, $CD31^-$, $CD45^-$, EdU^+ fraction (data not shown).

One additional question is whether activation status renders cells more proliferative. To address this topic, we compared the proliferation rate of activated fibroblasts (periostin lineage) [2] to resident fibroblast proliferation rates of cells identified by $PDGFR\alpha^{GFP+}$, $Col1a1\text{-}GFP^+$, or Tcf21 lineage-tagging. Between 5 and 9 days after permanent LAD ligation, periostin lineage tagged cells had comparable proliferation rates (Figure 7J) and numbers (Figure 7H) to the other three fibroblast lines, suggesting that there is not a subset of more proliferative, activated fibroblasts in the infarct zone.

3.9 Flow cytometry of proliferating cells after 7 days of isoproterenol treatment

We next compared the proliferative responses of the different cell populations with isoproterenol treatment by flow cytometry using both *PDGFRα*^{GFP} and *Col1a1-GFP* mouse lines with similar results for each. Proliferation and numbers of fibroblasts (GFP^+), endothelial cells ($CD31^+$), and pericytes ($CD31^-$, $CD45^-$, $CD146^+$) was observed while $CD45^+$ cell proliferation remained similar to basal levels (Figure 8C–D). It should be noted that fibroblast proliferation index by flow cytometry appears lower because all ventricular fibroblasts were examined by flow cytometry while only endocardial proliferation was quantified by histology. Similar to what we observed after MI, $CD146^+$ cells only represented 3–4% of the $CD31^-$, $CD45^-$, GFP^- population. Neither $Sca1^+$, $CD44^+$, nor $CD166^+$ cells represent any significant portion of the unidentified EdU^+ population (data not shown).

4. Discussion

Although recent studies have suggested that epicardial- and endocardial-derived fibroblasts constitute the majority of proliferating, fibrogenic cells after pressure overload [2, 8, 10], questions still remain regarding the responses of these resident fibroblasts during other disease processes. Here, we document the pattern and proliferation of resident fibroblast cells during perinatal heart growth, during homeostasis, and after injury. Taken together these data demonstrate that there are windows of opportunity for targeting the expansion of fibroblasts. Surprisingly, regardless of the injury type the peak of proliferation occurs around the first week after insult (Figure 9).

4.1 Patterns of expansion

Although increases in collagen deposition serve as a good approximation of fibroblast activation and accumulation, few reports illustrate fibroblast distribution throughout the heart. Use of fibroblast marking and lineage tracing affords a more discrete account of

fibroblast activity and permits fibroblast identification that precedes matrix deposition. At basal levels, adult cardiac fibroblasts were regularly dispersed between cardiomyocytes and concentrated in adventitial spaces. However, after injury collagen deposition represents more area than fibroblast area.

Within each mode of injury, a stereotypic pattern was observed, and collagen deposition overlapped extensively with fibroblast density. In hearts subjected to TAC, fibroblasts accumulated in both perivascular and random focal, interstitial areas. This pattern matches those described for collagen accumulation [37, 38]. It has been noted that as collagen density increases after pressure overload, collagen encircles cardiomyocytes and potentially disrupts force generation [39]. We observed that with chronic injury, fibroblasts also surrounded cardiomyocytes. With isoproterenol treatment, collagen accumulates predominantly in the endocardial regions [31, 32], and our results demonstrated that fibroblasts preferentially proliferated and amassed in this region. After permanent LAD ligation, the fibroblast pattern is consistent within the scar, however the size and area of each scar was variable, presumably due to the magnitude of ischemia and cardiomyocyte loss. Left atrial expansion of fibroblasts was variable with each injury. Others have observed that atrial remodeling is related to increased LV end diastolic pressure [40].

Previous studies have used αSMA as a label for activated fibroblasts, and after injury our fibroblast lines label a majority of the αSMA^{+} cells as determined by flow cytometry. However, there are remaining GFP^{+} fibroblasts that are not αSMA^{+}, suggesting that αSMA only labels a subset of these cells. After myocardial infarction fibroblasts in the infarct represented the largest proportion of GFP^{+} fibroblasts that were αSMA^{high}, while in areas of lower fibroblast expansion there was a continuum of αSMA expression. This continuum was recapitulated in injury models that also had lower fibroblast expansion. By IHC αSMA expression was not observed in every cell within the infarct zone, suggesting that flow cytometry may have a lower detection limit than IHC. These data indicate that our analyses were not limited to the fibroblasts that express αSMA and may provide a more comprehensive view of the resident cardiac fibroblast population.

It is also likely that after injury the Col1a1-GFP and $PDGFR\alpha^{GFP}$ reporters have different promoter activities. We do see an increase in GFP intensity after MI in the Col1a1-GFP line likely reflecting increased promoter activity (unpublished observation, MI). Thus, there remains a possibility that subsets of fibroblast exist that are differentially detected by these different reporters. We have yet to determine whether $Tcf21^{mCrem}$ lineage tracing efficiently labels endocardial-derived fibroblasts.

4.2 Proliferation of cardiac fibroblasts

Because identification of fibroblasts has been problematic, fibroblast proliferation is often determined indirectly and can be miscalculated. Frequently, fibroblast proliferation has been generalized to proliferation rates of non-myocytes [28, 41], morphological identification [42, 43], or primary fibroblast cultures [44–46].

4.2.1 Postnatal proliferation—A great deal of interest has been placed on perinatal cardiomyocyte proliferation, but few analyses have examined the proliferation of specific

populations of non-myocytes. Postnatal cardiomyocyte proliferation is limited to the first week after birth [15, 27, 47]. After this time heart size increases by cardiomyocyte hypertrophy [48]. One study of proliferation using rats observed a steady decrease in overall proliferation from postnatal day 3 to day 13 [28]. In contrast, we found that DNA synthesis increased between day 3 and day 7 and then dropped precipitously by 14 days after birth. Our data are in agreement with a rat study which observed decreased proliferation of fibroblasts and endothelial cells the first week after birth [49]. Interestingly, this pattern is similar to that observed in perinatal murine cardiomyocytes [15, 27, 47]. Both fibroblast and endothelial cell proliferation followed this overall trend suggesting a coordination of the signals that regulate proliferation. Decreases in proliferation were coincident with reported alterations in ECM [50] leaving a possibility that changes in the ECM may contribute to the regulation of proliferation. Approximately 0.4% of the fibroblasts were proliferating at any time in the adult mouse heart. This was considerably lower than the proliferation of immune and endothelial cells. These data are in agreement with the relative turnover rate of endothelial and mesenchymal cells in the human heart [51].

4.2.2 Proliferation after injury—One somewhat surprising result from our studies was that despite dramatically different profiles of fibroblast expansion, the peak of cell proliferation occurred within the very brief time window immediately following injury. Similar results have been observed in injury models of other species. While these studies often did not specify fibroblast proliferation, it was assumed that the majority of the cells proliferating were fibroblasts. For example, in canine hearts after ischemia reperfusion, peak proliferation rates of non-myocytes were observed within the first week of injury [52]; the majority of these cells were identified as myofibroblasts and endothelial cells [53]. Similarly, proliferation rates of non-myocytes in the mouse heart decreased to sham levels one month after pressure overload [54].

Our results from the Tcf21 lineage tagged fibroblasts are in agreement with other reports investigating fibroblast proliferation after TAC. Proliferation rates of connective tissue cells in the rat reportedly peaked at 7 days after constriction [42]. Similarly, non-myocyte proliferation in mice was shown to peak 7 days after TAC, which correlated with increased fibroblast numbers and collagen deposition. Non-myocyte proliferation decreased to sham levels 28 days later [54]. Using the *Col1a1-GFP* mouse line, fibroblast proliferation in lesion areas was 10–20% during the first 7 days after TAC, but by 4 weeks post-surgery the proliferation rate had dropped to below 5% [8]. Another study using flow cytometry reported that $CD90^+/Thy1^+$ fibroblasts had a basal proliferation index of 2.5% and 4 days after TAC the index reached ~10% and remained steady for up to 5 weeks [10]. One possible explanation for the discrepancy between our results and these results is that Thy1 may identify a subpopulation of fibroblasts that are more proliferative. Interestingly, when we compare adventitial to interstitial fibrosis we observe similar rates of proliferation. Moreover, when lesion proliferation is compared to non-lesion proliferation, we find that there is not a statistical difference. These data suggest that either the trophic factors leading to fibroblast proliferation are limiting or that signals inhibiting fibroblast proliferation arise after the first week of injury. Recruitment and activation of inflammatory cells are likely to be key in modulating fibroblast proliferation.

It is well established that isoproterenol exposure leads to cardiomyocyte death and that fibroblasts respond to this loss by expanding and depositing matrix. Previous reports have suggested that fibroblasts are the predominant proliferating cell population in this model of fibrosis [32]. Our results suggest that they constitute only 20–40% of the proliferating cells and, similar to pressure overload, peak proliferation rates occur within the first week of exposure. The proliferative cells are localized to the endocardium, as previously described, and proliferation reverts to basal levels within two weeks despite continuous exposure to isoproterenol. Unlike pressure overload and MI, fibroblast numbers do not continuously rise, indicating some form of fibroblast loss, possibly by apoptosis.

As replacement fibrosis is an essential element of survival after myocardial infarction, one would presume that fibroblast proliferation is rapid and robust. Indeed, we observed increases in fibroblast proliferation as early as 2 days post-MI. The expansion of fibroblasts was dramatic leading to 2–3 times more fibroblasts in the infarct area with proliferation rates returning toward basal levels as early as one week after ligation. These results are in agreement with those reported for myofibroblasts detected by αSMA expression. At 5 days post-MI, approximately 15% of myofibroblasts were proliferating, while endothelial cell proliferation at the same time was much lower [55]. By 7 days post-MI, myofibroblast proliferation was significantly decreased. Of interest is the observation that activated (periostin-expressing) fibroblasts have similar proliferation rates to the general fibroblast population. These data suggest that within the infarct there is not a specialized subset of proliferating fibroblasts and that these four mouse lines can be used to trace cardiac fibroblasts after injury. The results also demonstrate that after injury Tcf21 lineage and periostin lineage tagging can be useful in identifying fibroblasts in combination with other biologic readouts. Although it has been suggested that some fibroblasts undergo apoptosis after MI [56, 57], our data suggest that appreciable numbers of fibroblasts remain at least three weeks post-MI.

Although immune cells have been recognized as key elements in cardiac remodeling after MI [58–60], the relative ratios and cellular cross-talk of the non-myocyte populations after MI have not been described. Our data demonstrate that a greater than two-fold fibroblast (Col1a1-GFP^{+}) and four-fold immune cell (CD45^{+}) expansion occurs within five days post-MI and that fibroblasts and immune cells proliferate at similar rates. Together these two cell types constitute the majority of the proliferating cells during the proliferative phase described by Frangogiannis [61]. Others have observed that fibroblast and immune cell localization appear to be coordinated [62], but further analyses are required to understand how these cell populations influence each other. Together, these results suggest that a clear distinction between the inflammatory and fibroblast proliferative phase may not be as evident after MI.

5. Conclusions

Here, we present data delineating the location and expansion of the resident cardiac fibroblast population in the mouse. It is of note that all three fibroblast-specific mouse lines identify a uniform population which is also marked by the *POSTN*^{mCrem} lineage tag after fibroblast activation. These data inform experiments investigating both perinatal heart

regeneration and cardiac injury models. Regardless of the injury mechanism, general rates of proliferation and specifically, fibroblast proliferation, largely occur within the first week after experimental cardiac stress, suggesting that interventions targeted at fibroblast expansion would be most beneficial immediately after the insult.

Supplementary Material

Refer to Web version on PubMed Central for supplementary material.

Acknowledgments

We thank Taylor Rosengreen and Jocelyn Liu for their excellent technical support. We also thank Mingxin Tang in the Center for Cardiovascular Research Animal Physiology Core. This work was supported by NHLBI R01HLHL074257 (MDT), Chun Foundation (MDT), NHLBI Institutional Cardiology Training Grant T32 HL115505 (JTK and MJI), American Heart Association Grant PRE29630019 (JTK), and NHLBI 1F31HL126512 (MJI). The University of Hawaii Center for Cardiovascular Research Animal Physiology Core was supported by NIH grant P30 GM103341.

Abbreviations

GFP	green fluorescent protein
mCrem	mutated estrogen receptor P1 bacteriophage Cre recombinase
IB4	isolectin GS -IB_4
EdU	5-ethynyl-2-deoxyuridine
αSMA	alpha smooth muscle actin
ECM	extracellular matrix
MI	myocardial infarction
LAD	left anterior descending
TAC	transverse aortic constriction
IVS	interventricular septum
Col1a1	collagen type 1a1

References

1. Weber KT, Sun Y, Bhattacharya SK, Ahokas RA, Gerling IC. Myofibroblast-mediated mechanisms of pathological remodelling of the heart. Nat Rev Cardiol. 2013; 10:15–26. [PubMed: 23207731]
2. Kanisicak O, Khalil H, Ivey MJ, Karch J, Maliken BD, Correll RN, et al. Genetic lineage tracing defines myofibroblast origin and function in the injured heart. Nat Commun. 2016; 7:12260. [PubMed: 27447449]
3. Molkentin JD, Bugg D, Ghearing N, Dorn LE, Kim P, Sargent MA, et al. Fibroblast-Specific Genetic Manipulation of p38 MAPK in vivo Reveals its Central Regulatory Role in Fibrosis. Circulation. 2017
4. Kaur H, Takefuji M, Ngai C, Carvalho J, Bayer J, Wietelmann A, et al. Targeted Ablation of Periostin-Expressing Activated Fibroblasts Prevents Adverse Cardiac Remodeling in Mice. Circ Res. 2016

5. Gourdie RG, Dimmeler S, Kohl P. Novel therapeutic strategies targeting fibroblasts and fibrosis in heart disease. Nat Rev Drug Discov. 2016; 15:620–38. [PubMed: 27339799]
6. Gabbiani G. Evolution and clinical implications of the myofibroblast concept. Cardiovasc Res. 1998; 38:545–8. [PubMed: 9747425]
7. Stempien-Otero A, Kim DH, Davis J. Molecular networks underlying myofibroblast fate and fibrosis. J Mol Cell Cardiol. 2016; 97:153–61. [PubMed: 27167848]
8. Moore-Morris T, Guimaraes-Camboa N, Banerjee I, Zambon AC, Kisseleva T, Velayoudon A, et al. Resident fibroblast lineages mediate pressure overload- induced cardiac fibrosis. J Clin Invest. 2014; 124:2921–34. [PubMed: 24937432]
9. Pinto AR, Ilinykh A, Ivey MJ, Kuwabara JT, D'Antoni ML, Debuque R, et al. Revisiting Cardiac Cellular Composition. Circ Res. 2016; 118:400–9. [PubMed: 26635390]
10. Ali SR, Ranjbarvaziri S, Talkhabi M, Zhao P, Subat A, Hojjat A, et al. Developmental heterogeneity of cardiac fibroblasts does not predict pathological proliferation and activation. Circ Res. 2014; 115:625–35. [PubMed: 25037571]
11. Song K, Nam YJ, Luo X, Qi X, Tan W, Huang GN, et al. Heart repair by reprogramming non-myocytes with cardiac transcription factors. Nature. 2012; 485:599–604. [PubMed: 22660318]
12. Nag AC. Study of non-muscle cells of the adult mammalian heart: a fine structural analysis and distribution. Cytobios. 1980; 28:41–61. [PubMed: 7428441]
13. Doppler SA, Carvalho C, Lahm H, Deutsch MA, Dressen M, Puluca N, et al. Cardiac fibroblasts: more than mechanical support. J Thorac Dis. 2017; 9:S36–S51. [PubMed: 28446967]
14. Jiang J, Burgon PG, Wakimoto H, Onoue K, Gorham JM, O'Meara CC, et al. Cardiac myosin binding protein C regulates postnatal myocyte cytokinesis. Proc Natl Acad Sci U S A. 2015; 112:9046–51. [PubMed: 26153423]
15. Soonpaa MH, Kim KK, Pajak L, Franklin M, Field LJ. Cardiomyocyte DNA synthesis and binucleation during murine development. Am J Physiol. 1996; 271:H2183–9. [PubMed: 8945939]
16. Walsh S, Ponten A, Fleischmann BK, Jovinge S. Cardiomyocyte cell cycle control and growth estimation in vivo--an analysis based on cardiomyocyte nuclei. Cardiovasc Res. 2010; 86:365–73. [PubMed: 20071355]
17. Acharya A, Baek ST, Banfi S, Eskiocak B, Tallquist MD. Efficient inducible Cre-mediated recombination in Tcf21 cell lineages in the heart and kidney. Genesis. 2011; 49:870–7. [PubMed: 21432986]
18. Hamilton TG, Klinghoffer RA, Corrin PD, Soriano P. Evolutionary divergence of platelet-derived growth factor alpha receptor signaling mechanisms. Mol Cell Biol. 2003; 23:4013–25. [PubMed: 12748302]
19. Yata Y, Scanga A, Gillan A, Yang L, Reif S, Breindl M, et al. DNase I-hypersensitive sites enhance alpha1(I) collagen gene expression in hepatic stellate cells. Hepatology. 2003; 37:267–76. [PubMed: 12540776]
20. Madisen L, Zwingman TA, Sunkin SM, Oh SW, Zariwala HA, Gu H, et al. A robust and high-throughput Cre reporting and characterization system for the whole mouse brain. Nat Neurosci. 2010; 13:133–40. [PubMed: 20023653]
21. Acharya A, Baek ST, Huang G, Eskiocak B, Goetsch S, Sung CY, et al. The bHLH transcription factor Tcf21 is required for lineage-specific EMT of cardiac fibroblast progenitors. Development. 2012; 139:2139–49. [PubMed: 22573622]
22. Smith CL, Baek ST, Sung CY, Tallquist MD. Epicardial-derived cell epithelial-to-mesenchymal transition and fate specification require PDGF receptor signaling. Circ Res. 2011; 108:e15–26. [PubMed: 21512159]
23. Halfon S, Abramov N, Grinblat B, Ginis I. Markers distinguishing mesenchymal stem cells from fibroblasts are downregulated with passaging. Stem Cells Dev. 2011; 20:53–66. [PubMed: 20528146]
24. Carlson S, Trial J, Soeller C, Entman ML. Cardiac mesenchymal stem cells contribute to scar formation after myocardial infarction. Cardiovasc Res. 2011; 91:99–107. [PubMed: 21357194]
25. Bayes-Genis A, Soler-Botija C, Farre J, Sepulveda P, Raya A, Roura S, et al. Human progenitor cells derived from cardiac adipose tissue ameliorate myocardial infarction in rodents. J Mol Cell Cardiol. 2010; 49:771–80. [PubMed: 20713059]

26. Li F, Wang X, Capasso JM, Gerdes AM. Rapid transition of cardiac myocytes from hyperplasia to hypertrophy during postnatal development. J Mol Cell Cardiol. 1996; 28:1737–46. [PubMed: 8877783]
27. Hirai M, Chen J, Evans SM. Tissue-Specific Cell Cycle Indicator Reveals Unexpected Findings for Cardiac Myocyte Proliferation. Circ Res. 2016; 118:20–8. [PubMed: 26472817]
28. Banerjee I, Fuseler JW, Price RL, Borg TK, Baudino TA. Determination of cell types and numbers during cardiac development in the neonatal and adult rat and mouse. Am J Physiol Heart Circ Physiol. 2007; 293:H1883–91. [PubMed: 17604329]
29. Ieronimakis N, Hays A, Prasad A, Janebodin K, Duffield JS, Reyes M. PDGFRalpha signalling promotes fibrogenic responses in collagen producing cells in Duchenne Muscular Dystrophy. J Pathol. 2016
30. Tallquist MD, Molkentin JD. Redefining the identity of cardiac fibroblasts. Nat Rev Cardiol. 2017
31. Brooks WW, Conrad CH. Isoproterenol- induced myocardial injury and diastolic dysfunction in mice: structural and functional correlates. Comp Med. 2009; 59:339–43. [PubMed: 19712573]
32. Benjamin IJ, Jalil JE, Tan LB, Cho K, Weber KT, Clark WA. Isoproterenol-induced myocardial fibrosis in relation to myocyte necrosis. Circ Res. 1989; 65:657–70. [PubMed: 2527639]
33. Fatkhudinov T, Bolshakova G, Arutyunyan I, Elchaninov A, Makarov A, Kananykhina E, et al. Bone marrow-derived multipotent stromal cells promote myocardial fibrosis and reverse remodeling of the left ventricle. Stem Cells Int. 2015; 2015:746873. [PubMed: 25685158]
34. Williams SM, Golden-Mason L, Ferguson BS, Schuetze KB, Cavasin MA, Demos-Davies K, et al. Class I HDACs regulate angiotensin II-dependent cardiac fibrosis via fibroblasts and circulating fibrocytes. J Mol Cell Cardiol. 2014; 67:112–25. [PubMed: 24374140]
35. Squires CE, Escobar GP, Payne JF, Leonardi RA, Goshorn DK, Sheats NJ, et al. Altered fibroblast function following myocardial infarction. J Mol Cell Cardiol. 2005; 39:699–707. [PubMed: 16111700]
36. Talman V, Ruskoaho H. Cardiac fibrosis in myocardial infarction- from repair and remodeling to regeneration. Cell Tissue Res. 2016; 365:563–81. [PubMed: 27324127]
37. Brilla CG, Pick R, Tan LB, Janicki JS, Weber KT. Remodeling of the rat right and left ventricles in experimental hypertension. Circ Res. 1990; 67:1355–64. [PubMed: 1700933]
38. Weber KT, Brilla CG. Pathological hypertrophy and cardiac interstitium. Fibrosis and renin-angiotensin-aldosterone system. Circulation. 1991; 83:1849–65. [PubMed: 1828192]
39. Jalil JE, Doering CW, Janicki JS, Pick R, Shroff SG, Weber KT. Fibrillar collagen and myocardial stiffness in the intact hypertrophied rat left ventricle. Circ Res. 1989; 64:1041–50. [PubMed: 2524288]
40. De Jong AM, Van Gelder IC, Vreeswijk-Baudoin I, Cannon MV, Van Gilst WH, Maass AH. Atrial remodeling is directly related to end-diastolic left ventricular pressure in a mouse model of ventricular pressure overload. PLoS One. 2013; 8:e72651. [PubMed: 24039788]
41. Skosey JL, Zak R, Martin AF, Aschenbrenner V, Rabinowitz M. Biochemical correlates of cardiac hypertrophy. V. Labeling of collagen, myosin, and nuclear DNA during experimental myocardial hypertrophy in the rat. Circ Res. 1972; 31:145–57. [PubMed: 4261953]
42. Morkin E, Ashford TP. Myocardial DNA synthesis in experimental cardiac hypertrophy. Am J Physiol. 1968; 215:1409–13. [PubMed: 5723003]
43. Zak R. Development and proliferative capacity of cardiac muscle cells. Circ Res. 1974; 35(suppl II):17–26.
44. Burstein B, Libby E, Calderone A, Nattel S. Differential behaviors of atrial versus ventricular fibroblasts: a potential role for platelet-derived growth factor in atrial-ventricular remodeling differences. Circulation. 2008; 117:1630–41. [PubMed: 18347210]
45. Fredj S, Bescond J, Louault C, Delwail A, Lecron JC, Potreau D. Role of interleukin-6 in cardiomyocyte/cardiac fibroblast interactions during myocyte hypertrophy and fibroblast proliferation. J Cell Physiol. 2005; 204:428–36. [PubMed: 15717324]
46. Chilton L, Ohya S, Freed D, George E, Drobic V, Shibukawa Y, et al. K+ currents regulate the resting membrane potential, proliferation, and contractile responses in ventricular fibroblasts and myofibroblasts. Am J Physiol Heart Circ Physiol. 2005; 288:H2931–9. [PubMed: 15653752]

47. Alkass K, Panula J, Westman M, Wu TD, Guerquin-Kern JL, Bergmann O. No Evidence for Cardiomyocyte Number Expansion in Preadolescent Mice. Cell. 2015; 163:1026–36. [PubMed: 26544945]
48. Olivetti G, Anversa P, Loud AV. Morphometric study of early postnatal development in the left and right ventricular myocardium of the rat. II. Tissue composition, capillary growth, and sarcoplasmic alterations. Circ Res. 1980; 46:503–12. [PubMed: 6444555]
49. Reiss K, Cheng W, Kajstura J, Sonnenblick EH, Meggs LG, Anversa P. Fibroblast proliferation during myocardial development in rats is regulated by IGF-1 receptors. Am J Physiol. 1995; 269:H943–51. [PubMed: 7573538]
50. Williams C, Quinn KP, Georgakoudi I, Black LD 3rd. Young developmental age cardiac extracellular matrix promotes the expansion of neonatal cardiomyocytes in vitro. Acta Biomater. 2014; 10:194–204. [PubMed: 24012606]
51. Bergmann O, Zdunek S, Felker A, Salehpour M, Alkass K, Bernard S, et al. Dynamics of Cell Generation and Turnover in the Human Heart. Cell. 2015; 161:1566–75. [PubMed: 26073943]
52. Frangogiannis NG, Michael LH, Entman ML. Myofibroblasts in reperfused myocardial infarcts express the embryonic form of smooth muscle myosin heavy chain (SMemb). Cardiovasc Res. 2000; 48:89–100. [PubMed: 11033111]
53. Frangogiannis NG, Perrard JL, Mendoza LH, Burns AR, Lindsey ML, Ballantyne CM, et al. Stem cell factor induction is associated with mast cell accumulation after canine myocardial ischemia and reperfusion. Circulation. 1998; 98:687–98. [PubMed: 9715862]
54. Souders CA, Borg TK, Banerjee I, Baudino TA. Pressure overload induces early morphological changes in the heart. Am J Pathol. 2012; 181:1226–35. [PubMed: 22954422]
55. Virag JI, Murry CE. Myofibroblast and endothelial cell proliferation during murine myocardial infarct repair. Am J Pathol. 2003; 163:2433–40. [PubMed: 14633615]
56. Takemura G, Ohno M, Hayakawa Y, Misao J, Kanoh M, Ohno A, et al. Role of apoptosis in the disappearance of infiltrated and proliferated interstitial cells after myocardial infarction. Circ Res. 1998; 82:1130–8. [PubMed: 9633913]
57. Jose Corbalan J, Vatner DE, Vatner SF. Myocardial apoptosis in heart disease: does the emperor have clothes? Basic Res Cardiol. 2016; 111:31. [PubMed: 27043720]
58. Chen B, Frangogiannis NG. Immune cells in repair of the infarcted myocardium. Microcirculation. 2017; 24
59. Chen W, Frangogiannis NG. Fibroblasts in post-infarction inflammation and cardiac repair. Biochim Biophys Acta. 2013; 1833:945–53. [PubMed: 22982064]
60. Nahrendorf M, Pittet MJ, Swirski FK. Monocytes: protagonists of infarct inflammation and repair after myocardial infarction. Circulation. 2010; 121:2437–45. [PubMed: 20530020]
61. Frangogiannis NG. The mechanistic basis of infarct healing. Antioxid Redox Signal. 2006; 8:1907–39. [PubMed: 17034340]
62. Ruiz-Villalba A, Simon AM, Pogontke C, Castillo MI, Abizanda G, Pelacho B, et al. Interacting resident epicardium-derived fibroblasts and recruited bone marrow cells form myocardial infarction scar. J Am Coll Cardiol. 2015; 65:2057–66. [PubMed: 25975467]

Highlights

- Perinatal cardiac fibroblast proliferation parallels cardiomyocyte proliferation
- Resident cardiac fibroblasts expand in distinct patterns after cardiac injury
- Fibroblast proliferation peaks in the first week after injury, then returns to basal levels
- The fibroblast proliferative phase is similar to the reported inflammatory phase

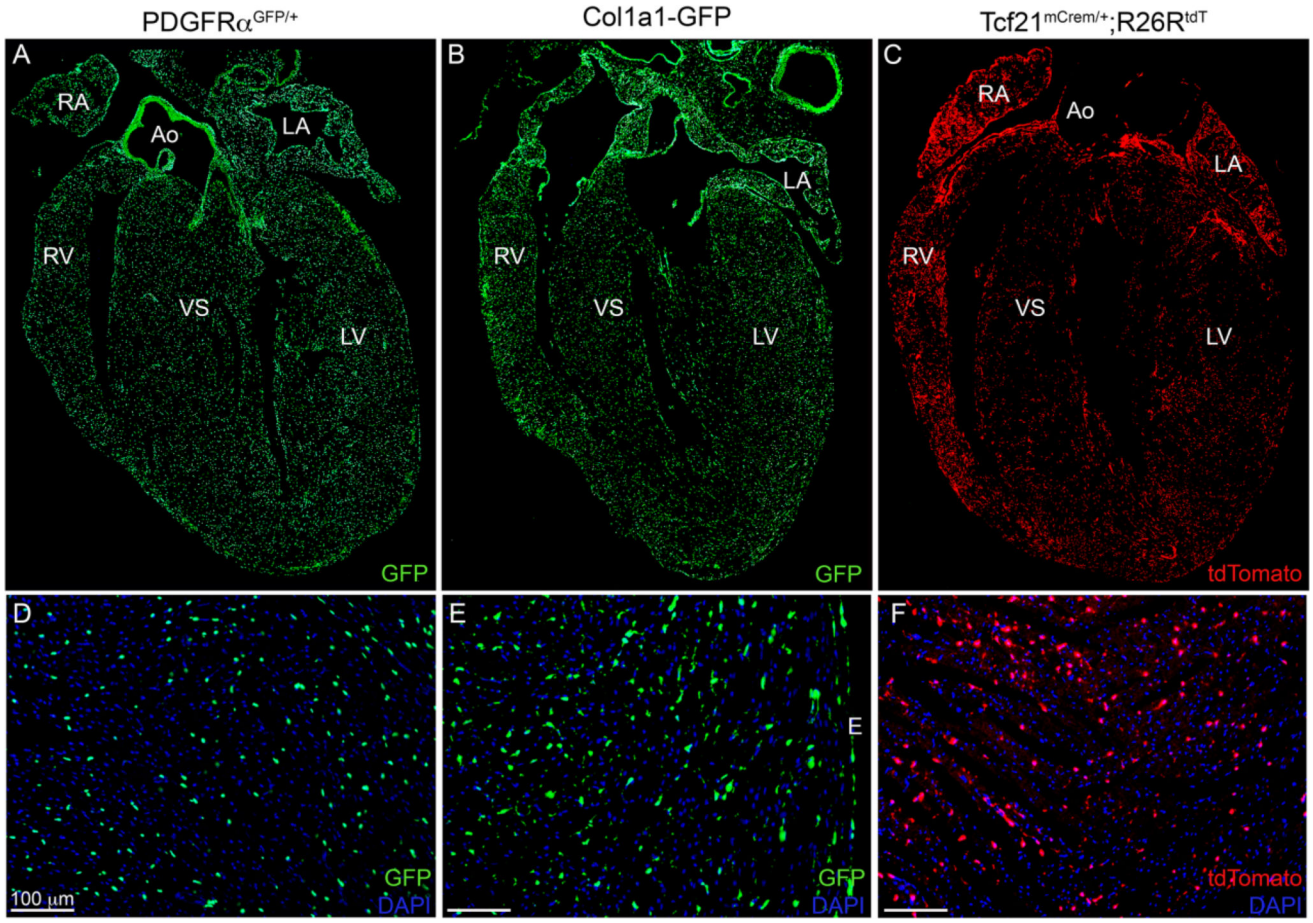

Figure 1. Fibroblast specific mouse lines

(**A–C**) 4 chamber view of (**A**) *PDGFRα*$^{GFP/+}$ (9 weeks), (**B**) *Col1a1-GFP* (25 weeks), and (**C**) *Tcf21*$^{mCrem/+}$*; R26R*^{tdT} (18 weeks) hearts. (**D–F**) Higher magnification of left ventricular free wall from different hearts. (**D**) *PDGFRα*$^{GFP/+}$ (5 weeks), (**E**) *Col1a1-GFP* (25 weeks) (**F**) *Tcf21*$^{mCrem/+}$*; R26R*^{tdT} (8 weeks). *Tcf21*$^{mCrem/+}$ mice were induced (**C**) for two weeks by tamoxifen chow (**F**) for two days by tamoxifen gavage. Ao: aorta; LA: left atria; RA: right atria; LV: left ventricle; RV: right ventricle; IVS: interventricular septum; E: epicardium. Scale bars: 100μm.

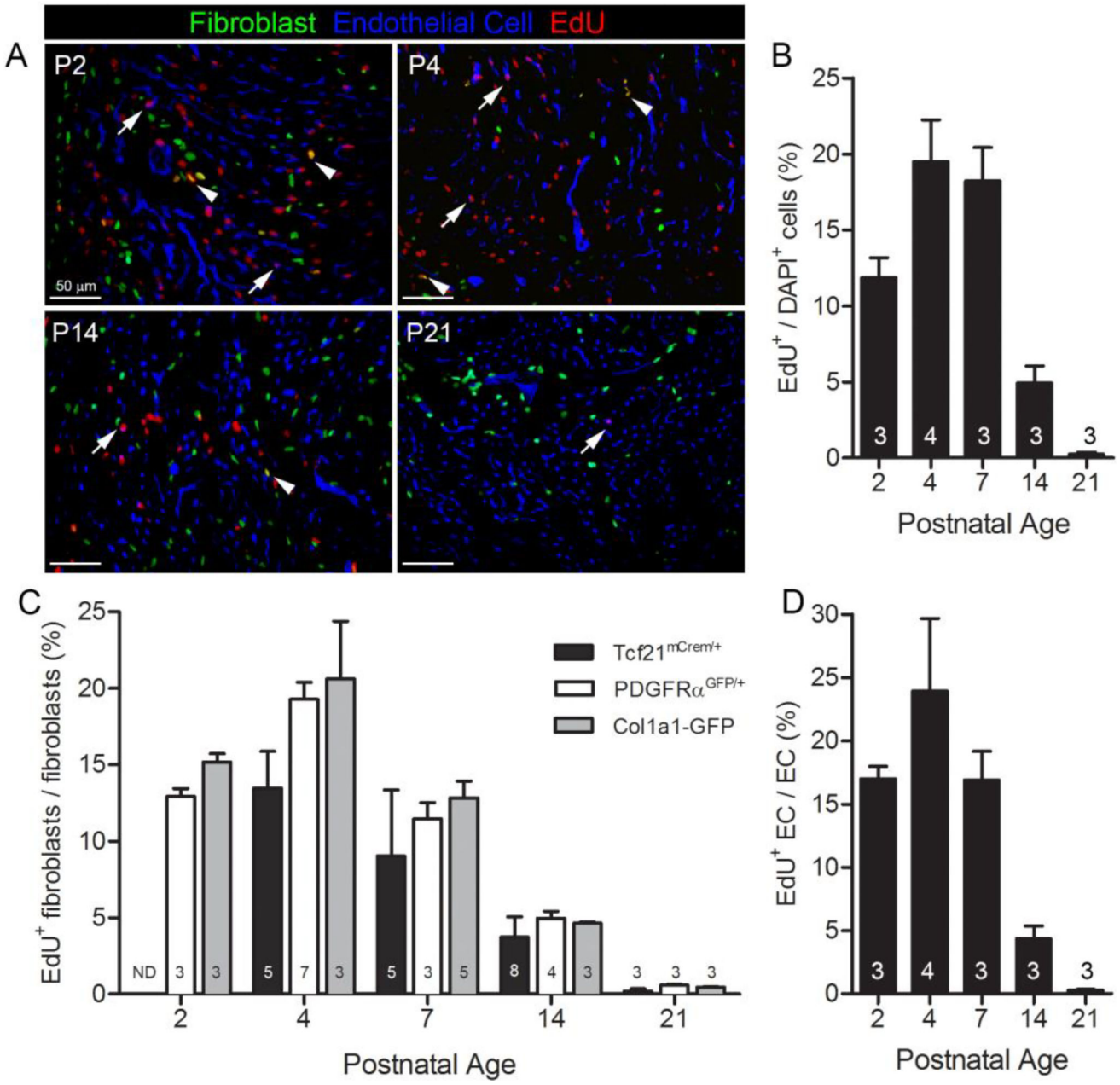

Figure 2. Fibroblast and endothelial cell proliferation in perinatal hearts

(**A**) Representative images at indicated postnatal time points. Fibroblasts: PDGFRα^{GFP} (green); endothelial cells: isolectin B4 (blue); and proliferating cells: EdU^{+} (red). Arrows indicate proliferating endothelial cells. Arrowheads indicate proliferating fibroblasts. (**B**) Overall proliferation rate of cells in *PDGFRα$^{GFP/+}$* hearts. (**C**) Quantification of proliferation index in PDGFRα^{GFP}, Col1a1-GFP, and Tcf21$^{mCrem/+}$;R26R^{tdT} labeled fibroblasts. (**D**) Postnatal endothelial cell proliferation index. ND: not determined. Numbers within bar graphs represent biological replicate n values. Results are mean ± SD. Scale bars: 50μm.

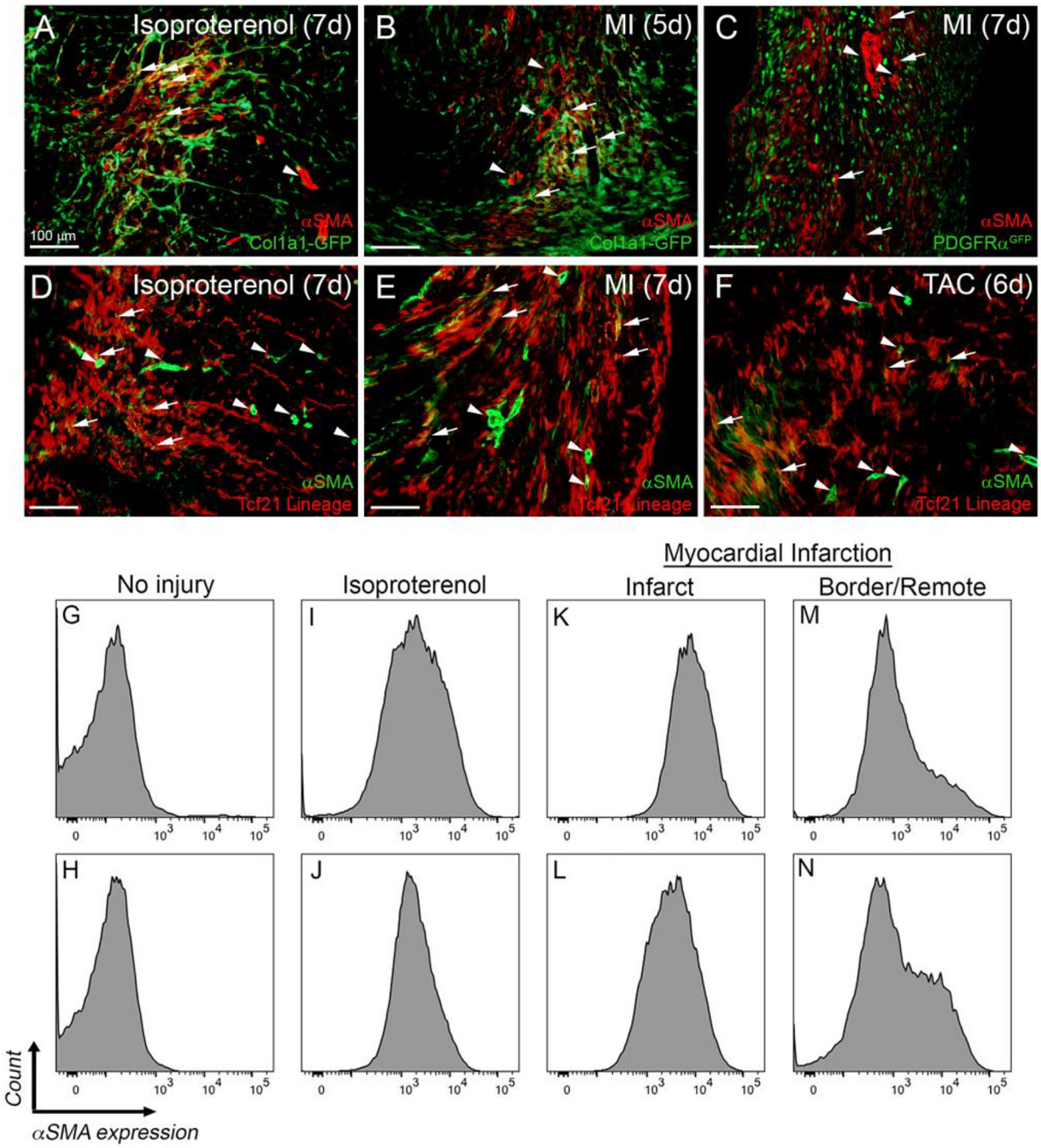

Figure 3. αSMA expression in fibroblast-tagged hearts after injury

(**A–B**) Representative images of αSMA staining in *Col1a1-GFP* hearts. (**C**) Representative images of αSMA staining in *PDGFRα*$^{GFP/+}$ hearts. (**D–F**) Representative images of αSMA staining in *Tcf21*$^{mCrem/+}$*; R26R*^{tdT} hearts. Arrows indicate examples of αSMA staining in fibroblasts identified by the indicated fluorescent tag. Arrowheads indicate a blood vessels with αSMA^{+} coronary vascular smooth muscle cells. Scale bars: 100μm. (**G–N**) Representative flow cytometry histograms of αSMA expression in GFP^{+} fibroblasts isolated from (**G, I, K, M**) *Col1a1-GFP* and (**H, J, L, N**) *PDGFRα*$^{GFP/+}$ hearts at (**G–H**) baseline,

(**I–J**) after 7 days of isoproterenol injections, and 5 days after MI (**K–L**) in the infarct and (**M–N**) border/remote area.

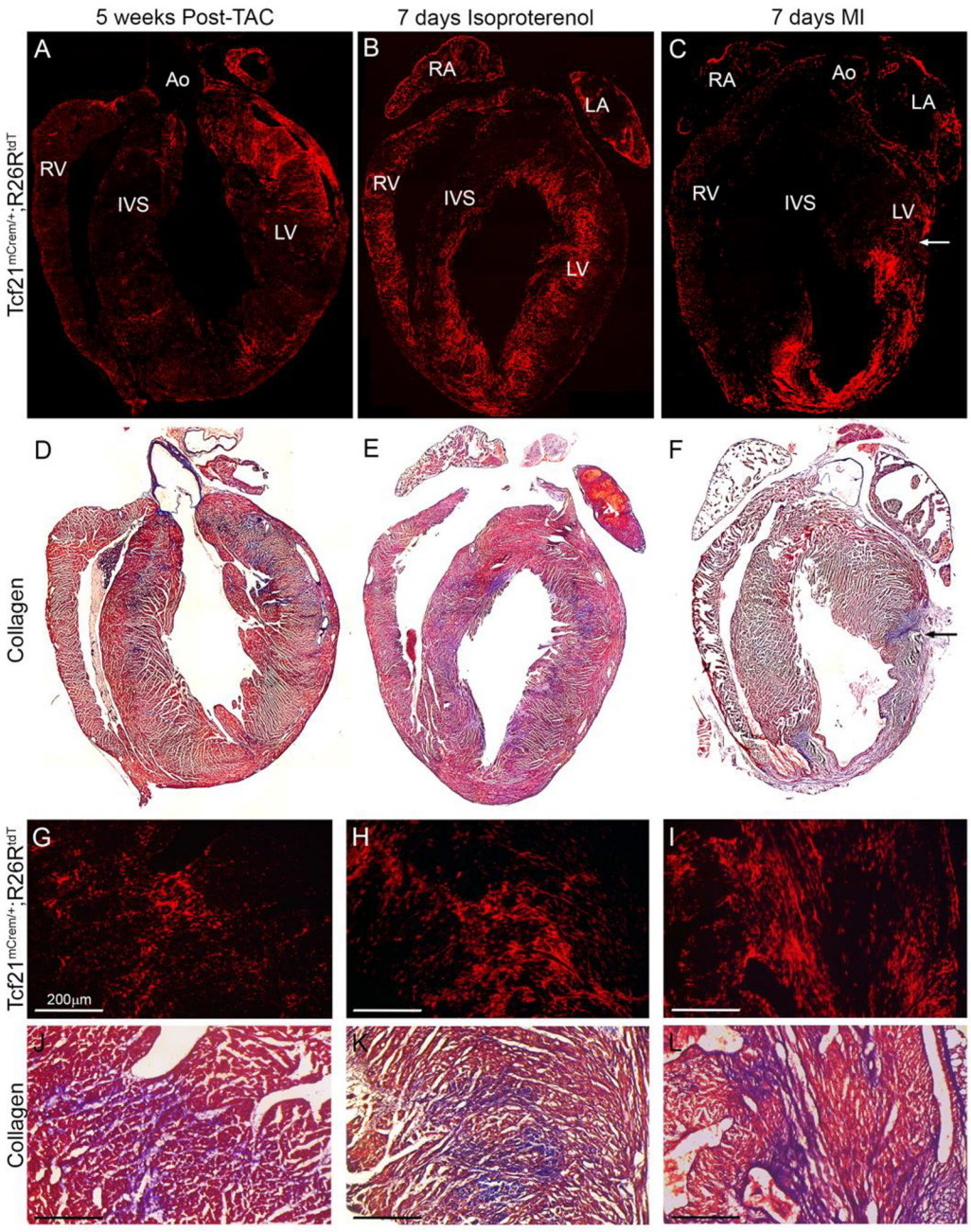

Figure 4. Tcf21 lineage tagged cells and collagen deposition after injury

(**A–C**) 4 chamber view of Tcf21 lineage tagged cells (red) at the indicated time points of injury. (**D–F**) 4 chamber view of Gomori's trichrome staining of hearts in A–C. (blue: collagen deposition) Arrow indicates the suture site. (**G–I**) Higher magnification of Tcf21 lineage tagged cells and (**J–L**) Gomori's trichrome staining of adjacent sections of (G–I) (blue: collagen deposition). Ao: aorta; LA: left atria; RA: right atria; LV: left ventricle; RV: right ventricle; IVS: interventricular septum. Scale bars: 200μm.

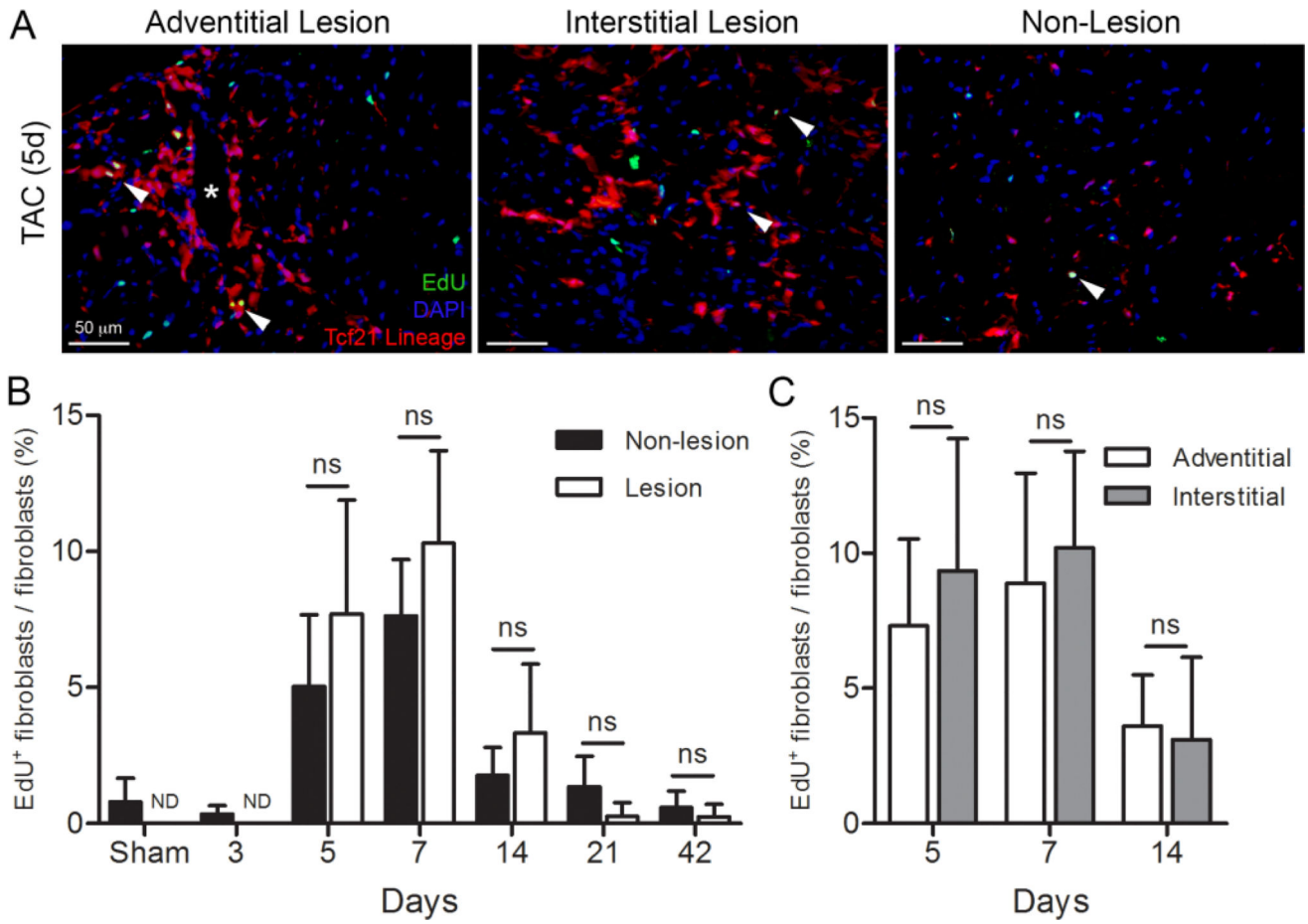

Figure 5. Fibroblast proliferation after pressure overload

(**A**) Representative images of an adventitial, interstitial lesion, and a non-lesion area in a *Tcf21*$^{mCrem/+}$*; R26R*^{tdT} heart 5 days after transverse aortic constriction (TAC). Fibroblasts: tdTomato (red); nuclei: DAPI (blue), and proliferating cell: EdU^{+} (green). Arrowheads indicate proliferating fibroblasts. Asterisk indicates a blood vessel. (**B**) Quantification of percent fibroblast proliferation in lesion and non-lesion areas. (**C**) Quantification of percent fibroblast proliferation in adventitial and interstitial lesions. n=3–5 mice per group. ND: not determined. ns: not significant; unpaired student's t-test. Results are mean ± SD. Scale bars: 50μm.

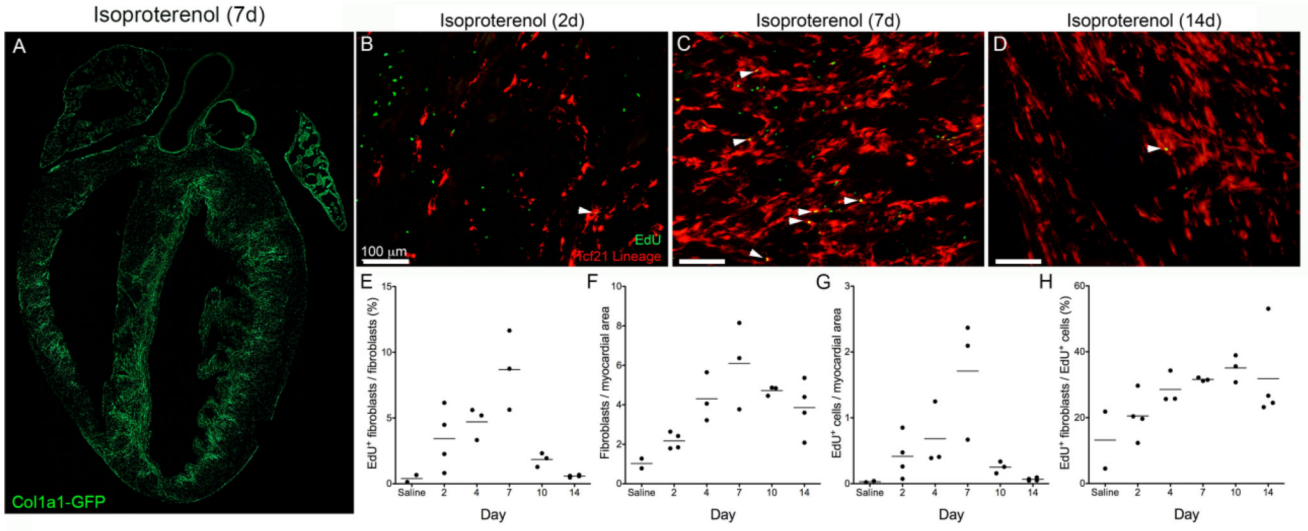

Figure 6. Fibroblast proliferation after isoproterenol injection

(**A**) Four chamber view of endocardial fibroblast expansion 7 days of isoproterenol treatment in a *Col1a1-GFP* heart. Fibroblasts: GFP (green). (**B–D**) Tcf21 lineage tagged fibroblasts and EdU labeled proliferating cells after (**B**) 2, (**C**) 7 and (**D**) 14 days of isoproterenol injections. Fibroblasts: tdTomato (red); proliferating cell: EdU (green). Arrowheads indicate proliferating fibroblasts. (**E**) Percent of proliferating fibroblasts, (**F**) number of fibroblasts, (**G**) number of proliferating cells, (**H**) percent of proliferating cells that are fibroblasts. All quantifications were a minimum of five fields of view from two non-sequential sections in at least two biologic replicates and were normalized to myocardial area where applicable. Each point represents the average of one biological replicate. Scale bars: 100μm.

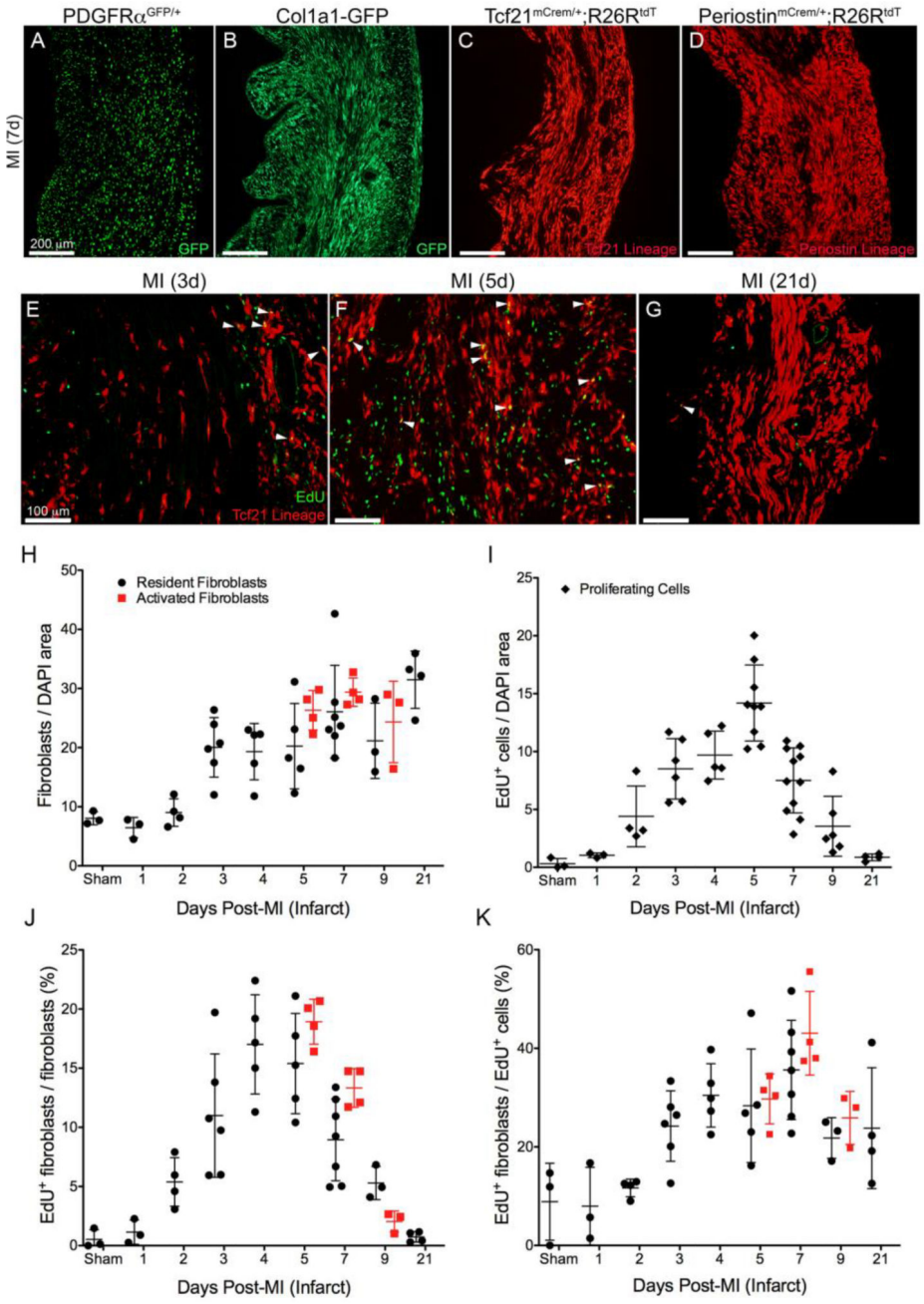

Figure 7. Fibroblast proliferation after myocardial infarction

Resident fibroblast expansion in left ventricular free wall 7 days after LAD ligation using fibroblast lines (**A**) *PDGFRα*^{GFP}, (**B**) *Collagen1a1-GFP*, (**C**) *Tcf21*$^{mCrem/+}$; *R26R*^{tdT} or (**D**) *POSTN*$^{mCrem/+}$; *R26R*^{tdT}. (**E–G**) Proliferation of Tcf21 lineage-tagged fibroblasts (**E**) 3 days post-MI, (**F**) 5 days post-MI and (**G**) 21 days post-MI. Fibroblasts: tdTomato (red); proliferating cell: EdU (green). Arrowheads indicate proliferating fibroblasts. (**H**) Number of fibroblasts (**I**) number of proliferating cells (**J**) percent of fibroblasts that are proliferating and (**K**) percent of proliferating cells that are fibroblasts. Resident fibroblasts: PDGFRα^{GFP}, Collagen1a1-GFP or Tcf21 lineage (black circles); activated fibroblasts: periostin lineage

(red squares); proliferating cell: EdU^+ (black diamonds). Results are mean ± SD. Each point represents the average of one biological replicate normalized to nuclear area where applicable. Scale bars: (A–D) 100μm and (E–G) 200μm.

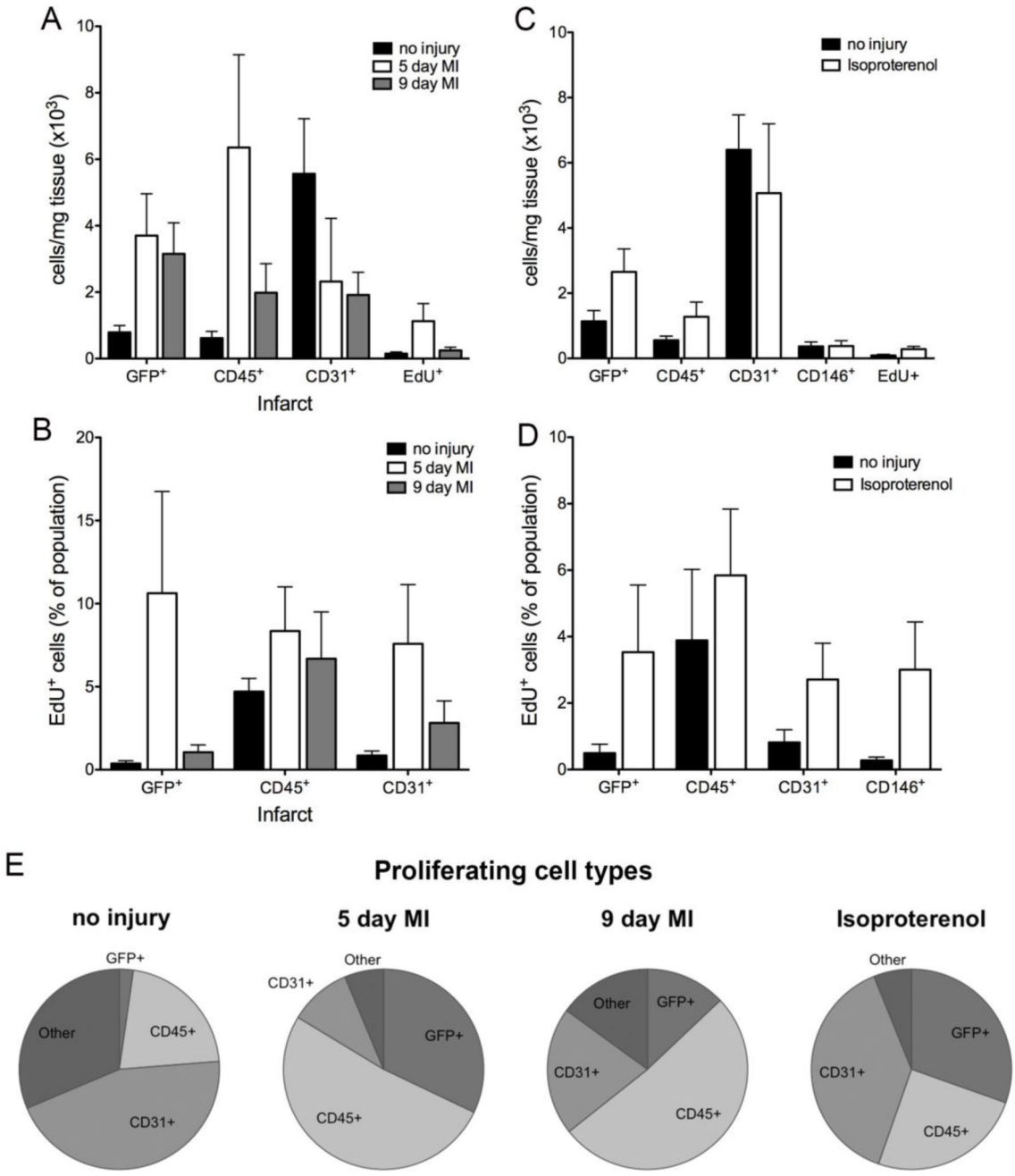

Figure 8. Flow cytometry of cell populations after injury

(**A, C**) Cell numbers determined by flow cytometry after (**A**) myocardial infarction (infarct) or (**C**) isoproterenol treatment (day 7; both ventricles). (**B, D**) Proliferation by cell type after (**B**) myocardial infarction (infarct) or (**D**) isoproterenol treatment (day 7; both ventricles). For no injury, left ventricle was isolated in the MI controls, and both ventricles were isolated for isoproterenol controls. (**E**) Distribution of each cell type within the proliferating cell population after the indicated treatments. Proliferating cell: EdU^+; immune cell: $CD45^+$; endothelial cell: $CD31^+$; pericyte: $CD146^+/CD31^-/CD45^-/GFP^-$; other: $CD31^-/CD45^-/GFP$

$^{-}$; fibroblast: Col1a1-GFP^{+} (MI) and Col1a1-GFP^{+} or PDGFRα^{GFP+} cells (isoproterenol). n=4–6 mice per group. Results are mean ± SD.

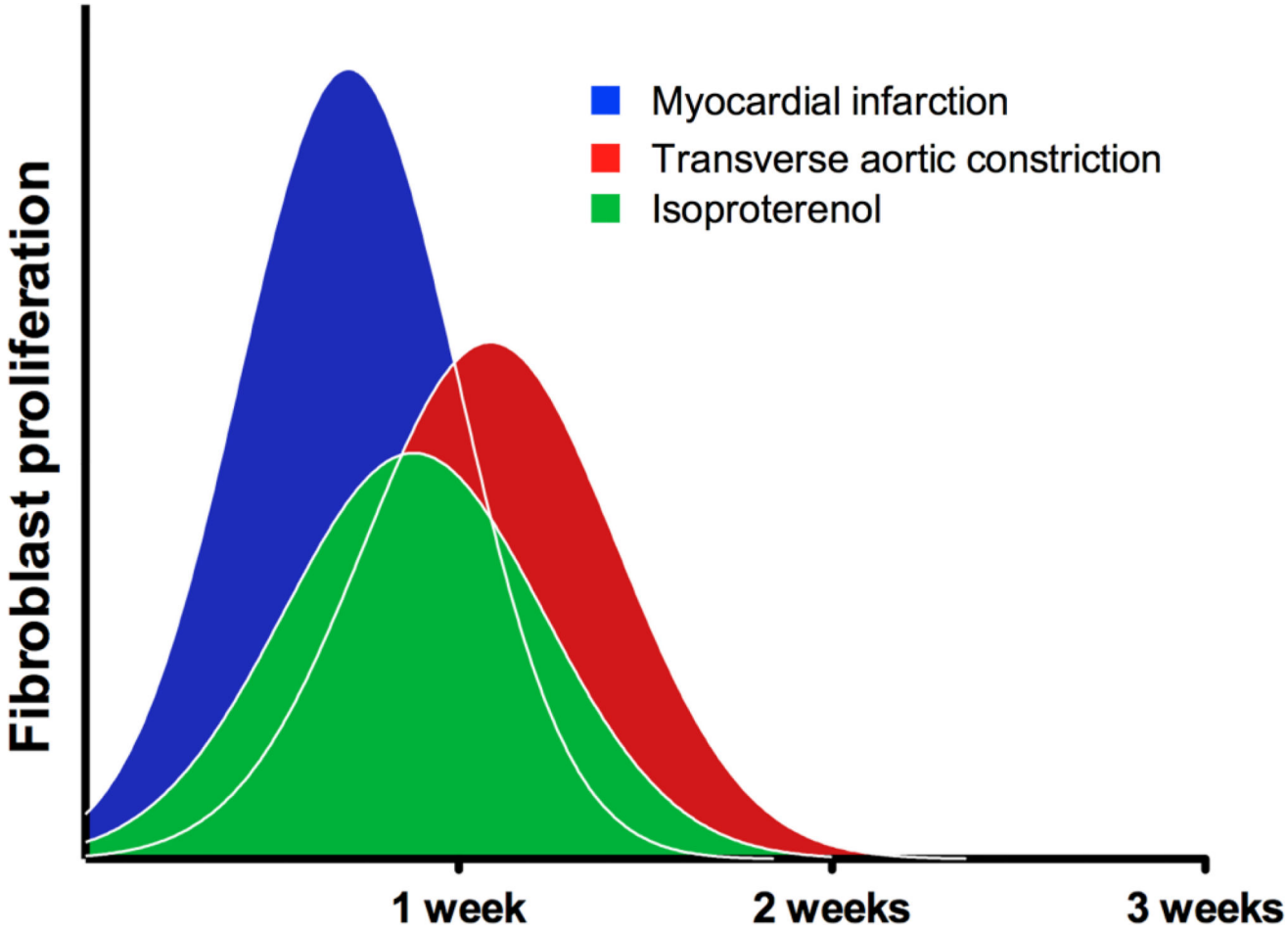

Figure 9. Fibroblast proliferation profiles after injury

Schematic of fibroblast proliferation suggesting general patterns of proliferation after injury. Within these experimental parameters peak fibroblast proliferation is around the first week after injury and rapidly returns to basal levels.